

Inversion of Band Patterns in Spherical Tumblers

Pengfei Chen,¹ Bryan J. Lochman,² Julio M. Ottino,^{1,2,3} and Richard M. Lueptow^{2,*}

¹Department of Chemical and Biological Engineering, Northwestern University, Evanston, Illinois 60208, USA

²Department of Mechanical Engineering, Northwestern University, Evanston, Illinois 60208, USA

³The Northwestern Institute on Complex Systems (NICO), Northwestern University, Evanston, Illinois 60208, USA

(Received 29 September 2008; published 6 April 2009)

Bidisperse granular mixtures in spherical tumblers segregate into three bands: one at each pole and one at the equator. For low fill levels, large particles are at the equator; for high fill levels, the opposite occurs. Segregation is robust, though the transition depends on fill level, particle size, and rotational speed. Discrete element method simulations reproduce surface patterns and reveal internal structures. Particle trajectories show that small particles flow farther toward the poles than large particles in the upstream portion of the flowing layer for low fill levels leading to a band of small particles at each pole. The opposite occurs for high fill levels, though more slowly.

DOI: 10.1103/PhysRevLett.102.148001

PACS numbers: 45.70.Mg, 45.70.Qj

Granular materials, a prototype complex system far from equilibrium [1,2], exhibit fascinating collective features. For example, bidisperse mixtures of small and large particles in long rotating cylindrical tumblers, which are used in applications ranging from foodstuffs to mining to cement processing, segregate after $O(10)$ to $O(100)$ rotations into bands of small and large particles with a wavelength of about one tumbler diameter [3] under a wide range of conditions [4–10]. Though the onset mechanism is unclear, large particles first segregate near the flat end walls of the tumbler [3,8,11]. In half full spherical tumblers, an alternative end wall configuration, large particles accumulate near the poles with a band of small particles at the equator [12]. The inversion of this pattern for other fill levels, which does not occur in cylindrical tumblers [13], is the topic of this Letter.

We consider bidisperse spherical glass particles in a clear acrylic spherical container with diameter $D = 14$ cm. Three parameters were varied: (1) particle sizes (mm): 1 + 2, 1 + 3, 1 + 4, and 2 + 4 (equal bulk volumes of small black particles [d_S] and large clear particles [d_L]); (2) rotation rates for a flat, continuously flowing layer: 2, 5, 10, 20, and 30 rpm; and (3) fill levels: 20%–60% by bulk volume measured using a graduated cylinder. Before loading the particles, the tumbler was sprayed with an antistatic aerosol (McMaster-Carr, Chicago, IL). Because mixtures pack more densely than monodisperse particles, several iterations were necessary to reach the desired initial fill level. Images were obtained at 102 rotations, assuring a steady surface segregation pattern.

Unlike previous work [12], a second segregation pattern appears at the top free surface depending on the fill level. The small-large-small (“SLS”) pattern in Fig. 1(a) has a center band of large particles bounded by outer bands of small particles. It occurs at low fill levels within 5–10 rotations. The reverse pattern, “LSL” in Fig. 1(b), occurs at high fill levels [12], but requires >20 rotations to be-

come clear. In both cases, the particles also segregate radially with the small particles forming the radial core. In fact, the radial core of small particles for LSL extends to the pole regions [Fig. 1(c)].

The axial segregation patterns (top view) and transition depend on fill level, particle size ratio, and absolute size of particles (Fig. 2). The transition between patterns is gradual. For fill levels just below the transition, a weak SLS pattern is observed; just above the transition a weak LSL pattern occurs. The transition fill level increases with the large particle size when the small particle size is fixed (left three columns of Fig. 2). For the same size ratio, the 2 + 4 mm mixture has a much higher transition fill level than the 1 + 2 mm mixture, indicating that the particle sizes themselves also affect the transition fill level.

For most cases increasing the rotation rate brings on axial segregation more quickly and enhances the degree of segregation, but does not affect the surface pattern [Fig. 3(a)]. But for fill levels above 50%, the surface segregation pattern changes from LSL to SLS with increasing rotation rate [Fig. 3(b)] as the rotation rate increases from 10 to 20 rpm in this case. The only transition that

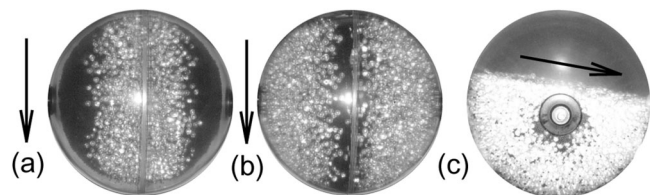


FIG. 1. Two surface segregation patterns occur for 1 mm black (S) and 4 mm clear (L) glass beads at 20 rpm. (a) Top view: SLS, 30% full, (b) top view: LSL, 60% full. The narrow vertical stripe on the tumbler is the seam between its two halves. (c) Side view after removing the tumbler from the apparatus: 60% full. The circle at the pole is the suction cup for connection to a shaft. Flow is indicated by arrows.

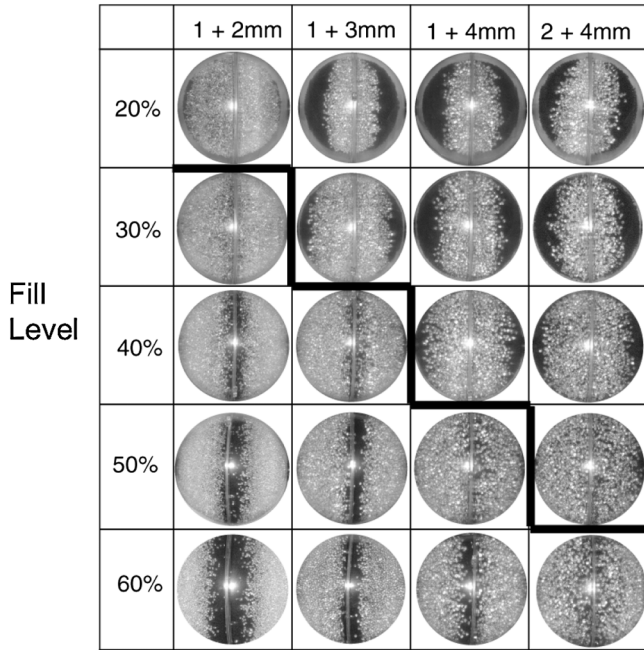


FIG. 2. The SLS segregation pattern occurs at low fill levels (above bold line) while the LSL pattern occurs at high fill levels at 20 rpm (flow is top to bottom).

occurs with increasing rotation rate is from LSL to SLS; no transitions from SLS to LSL were observed.

To investigate the origin of the segregation patterns, we simulated the flow of the 2 + 4 mm mixture in a $D = 14$ cm sphere using the discrete element method [14] with 24 695–74 080 particles, depending on fill level. As in our previous simulations [15], the linear-spring dashpot force model was used for the normal force between contacting particles [16]. A tangential force model without a memory effect [17,18] was used, since it produces the correct macroscopic segregation pattern and is more efficient. The material properties of glass were used (2500 kg/m³, 0.97 restitution coefficient, 0.6 coefficient of friction for particles and the smooth tumbler wall).

The simulations successfully reproduce the experimental steady-state segregation patterns, as shown in Fig. 4, as well as slight slip between the body of particles and the

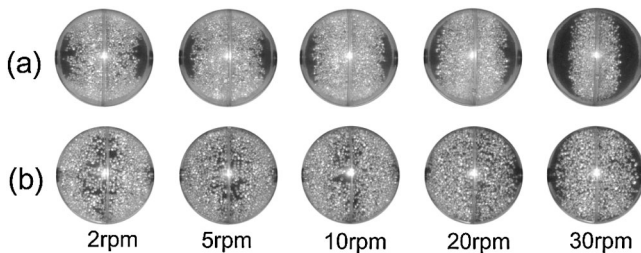


FIG. 3. (a) The degree of SLS segregation depends on the rotation rate for 1 + 3 mm particles at 30% full. (b) The segregation pattern changes from LSL to SLS increasing from 10 to 20 rpm for the 2 + 4 mm particles at 50% full.

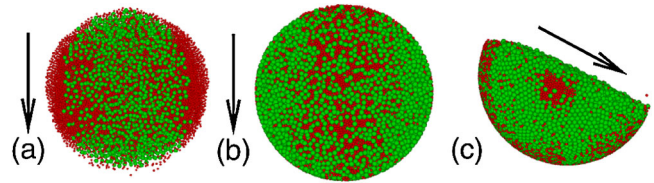


FIG. 4 (color online). Segregation after 100 rotations at 20 rpm for 2 + 4 mm particles in a 14 cm tumbler: (a) SLS, 20% full; (b) LSL, 60% full; (c) LSL pole region.

wall at low fill levels. As in the experiments, the SLS pattern in Fig. 4(a) occurs faster and is sharper than the LSL pattern in Fig. 4(b). Figure 4(c) shows the radial core extending to the pole regions, evident experimentally [Fig. 1(c)]. (Angles of repose cannot be compared because the tumbler was removed from the apparatus in Fig. 1(c).) Slices of the internal structure for fully developed segregation are shown in Fig. 5. Similar to the axial segregation in cylindrical tumblers [10,13,19], bands of small particles in spherical tumblers result from the expansion of the core of small particles to the free surface. For SLS, the core of relatively pure small particles extends the length of the tumbler parallel to the axis of rotation. For LSL, the core of small particles is less pure, and it reaches the free surface at the equator of the tumbler ($z = 0$), though percolation results in some large particles also reaching the flowing layer surface.

To probe the internal structure of the fully developed segregation, the local concentration of small particles [$C_s(x, y, z)$] was calculated over the computational domain (using 20 bins in each dimension) over $2/3$ tumbler rotation to provide adequate time to average out randomness while still achieving adequate time resolution. From this, the regions of small and large particles can be displayed as particle concentration isosurfaces. In Fig. 6(a) for SLS, the core of small particles extends parallel to the axis of rotation but is narrow at the equator of the tumbler and fills the pole regions. Large particles surround the narrowed core of small particles at the equator [Fig. 6(c)]. For LSL, the core of small particles is much larger at the

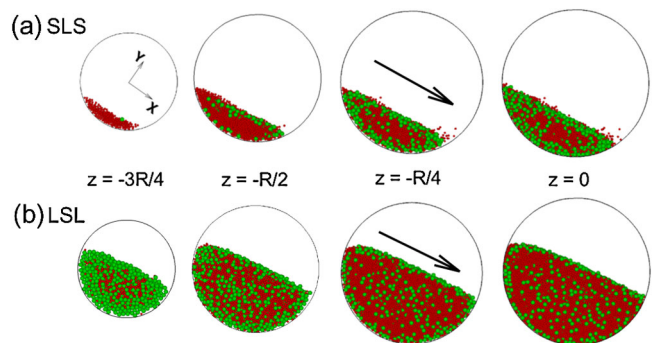


FIG. 5 (color online). Snapshots of slices at different axial positions after the segregation has reached steady state.

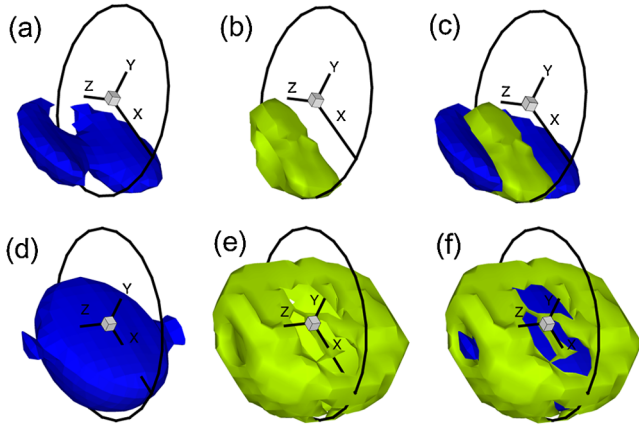


FIG. 6 (color online). Steady state small and large particle regions. SLS: (a) small particle region, $C_s \geq 0.75$; (b) large particle region, $C_s \leq 0.3$; (c) combined regions. LSL: (d) small particle region, $C_s \geq 0.5$; (e) large particle region, $C_s \leq 0.3$; (f) combined regions.

equator [Fig. 6(d)] but narrows near the poles. The large particles surround the small particles except at the equator and poles [Fig. 6(f)].

Figure 7 shows the evolution of segregation in terms of the concentration of small particles averaged over transverse cross sections $[C_s(z)]$. The high degree of symmetry about the equator demonstrates the quality of the simulations. For SLS, Fig. 7(a), small particles have an initial uniform concentration of $C_s(z) = 0.5$, but quickly accumulate at the poles at a rate similar to radial segregation reaching nearly 1.0 within the first 2/3 rotation. By seven rotations, the concentration is nearly at steady state, and the bands of small particles at the poles are quite pure. At the equator, the small particle concentration of 0.4 at steady state represents the core of small particles surrounded by large particles. For LSL, Fig. 7(b), the evolution of the segregation is much slower, reaching steady state after 30 tumbler rotations (not shown). The high small particle concentration at the poles is due to the core of small particles extending right to the poles [Figs. 1(c) and 4(c)]. A

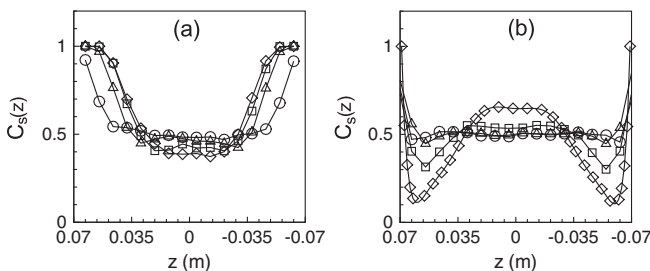


FIG. 7. Concentration of small particles along the axial length for (a) SLS and (b) LSL. \circ , initial (0–2/3 rotation); \triangle , (8/3–10/3 rotations); \square , (20/3–22/3 rotations); \diamond , full segregation (100 rotations). Standard deviations are 0.002–0.040 except at the poles during the transient.

short distance from the poles, large particles dominate, corresponding to the neck in the small particle concentration in Fig. 6(d). The concentration near the equator is not pure due to imperfect segregation [Fig. 5(b)]. For both patterns, the segregation starts at the poles and propagates to the equator.

To understand the evolution of axial segregation, we tracked particles starting in two small regions near the upstream end of the flowing layer: region A, on the surface of the flowing layer at the steady-state boundary between small and large particle bands for SLS; region B, half way between A and the equator. Identical locations were used for LSL. Ensemble average particle paths for 20–150 particles are shown in Fig. 8. During the initial rotations for the SLS pattern, both types of particles drift toward the poles in the upstream portion of the path and back toward the equator in the downstream portion, but small particles travel farther toward the poles and do not return back as far toward the equator as large particles. The particle paths end where the particles stop flowing (on average) and are trapped in solid body rotation. Thus, small particles are trapped farther from the equator than where they start, and large particles are trapped closer to the equator, producing the SLS pattern. The trajectories of the small particles are shorter because they percolate through the large particles and fall out of the flowing layer sooner. The deviation of two particle paths persists until the final fully segregated state appears when particles simply flow down the slope and return to their original axial position.

For the LSL pattern, in which large particles accumulate at the end walls as in cylindrical tumblers, the paths for the two particle types initially overlay each other. During segregation, large particles drift slightly toward the poles

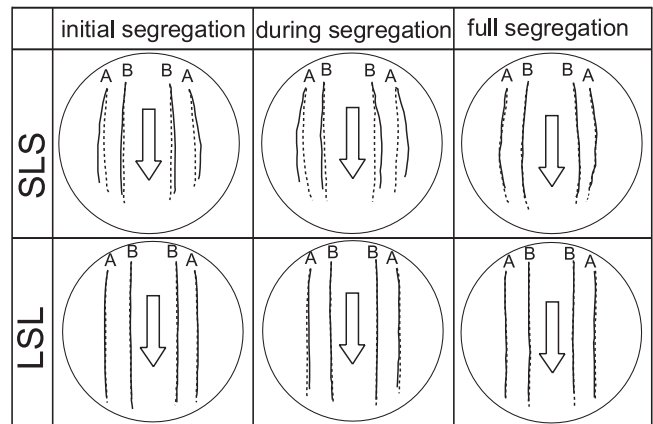


FIG. 8. Ensemble averaged trajectories of 2 mm (solid line) and 4 mm (dashed line) particles starting on the free surface: initial (0–2/3 rotation); during segregation (8/3–10/3 rotations); and full segregation (100 rotations). Standard deviations in horizontal position at the path beginning due to sampling are $<2d_s$ and $<0.8d_L$ for small and large particles; at the path end the values increase to $<5d_s$ and $<1.6d_L$ for SLS and $<2.5d_s$ and $<1.3d_L$ for LSL due to diffusion.

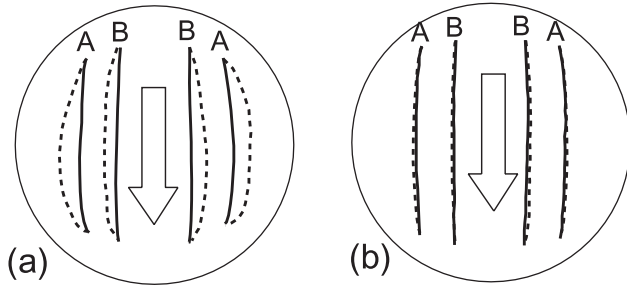


FIG. 9. Trajectories of the 2 mm (solid line) and 4 mm (dashed line) particles on the free surface for monodisperse systems at (a) 20% full and (b) 60% full. *A* and *B* are the same as in Fig. 8.

compared to small particles. Again, at steady state the deviation between the two paths disappears. Deviations between the paths for LSL are small compared to SLS, so segregation occurs more slowly.

For comparison, Fig. 9 shows the flow of monodisperse systems rotated under the same conditions as in Fig. 8. For the high fill level [Fig. 9(b)], the trajectories are similar to the bidisperse case (LSL in Fig. 8). For the low fill level [Fig. 9(a)], the trajectories of large particles curve more toward the poles than those of small particles, opposite of the bidisperse case. Simulations of monodisperse particles in a smaller 7 cm diameter tumbler indicate that the curvature of the path is inversely related to D/d . Thus, larger particles have more curved paths than small particles for the same tumbler diameter.

The presence of two particle species changes the trajectories at low fill levels but not at high fill levels because strongly curved trajectories are associated with low fill levels in both cases. Experiments and simulations show that at low fill levels a monolayer one or two particles high stacks up on the tumbler wall at the upstream end of the flowing layer during the initial segregation due to the obtuse angle between the tumbler wall and flowing layer. For monodisperse systems, the particles tend to fall out of the monolayer along the tumbler wall (toward the poles) resulting in a curved trajectory. Because of smaller D/d , large particles arc farther toward the poles than small particles [Fig. 9(a)]. For bidisperse systems, the monolayer is nearly all small particles which fall toward the poles, thus directing larger particles toward the equator leading to the SLS trajectories in Fig. 8. When the tumbler is more than 50% full for both monodisperse and bidisperse systems, the monolayer does not occur due to the acute angle between the tumbler wall and the flowing layer. The particle trajectories are nearly straight with a slightly greater

tendency for larger particles to flow toward the poles (as in the monodisperse case) leading to the LSL trajectories in Fig. 8.

While this work has isolated some aspects of axial segregation in a spherical tumbler, many details are not understood, including the impact of tumbler size and particle size on the transition from SLS to LSL with changing fill levels and rotational speeds. Likewise the driving force for axial segregation deserves further investigation, particularly the role of the monolayer on the wall at the upstream end of the flowing layer, which appears to initiate and drive the segregation. Similar patterns occur for granular systems wholly immersed in water whose internal structures were studied with NMR [20].

*r-lueptow@northwestern.edu

- [1] H. M. Jaeger and S. R. Nagel, *Science* **255**, 1523 (1992).
- [2] J. M. Ottino, *Chem. Eng. Sci.* **61**, 4165 (2006).
- [3] G. Juarez, J. M. Ottino, and R. M. Lueptow, *Phys. Rev. E* **78**, 031306 (2008).
- [4] Y. Oyama, *Bull. Inst. Phys. Chem. Res. (Tokyo)* **18**, 600 (1939).
- [5] M. B. Donald and B. Roseman, *Br. Chem. Eng.* **7**, 749 (1962).
- [6] M. Nakagawa, *Chem. Eng. Sci.* **49**, 2540 (1994).
- [7] O. Zik, D. Levine, S. G. Lipson, S. Shtrikman, and J. Stavans, *Phys. Rev. Lett.* **73**, 644 (1994).
- [8] K. M. Hill and J. Kakalios, *Phys. Rev. E* **49**, R3610 (1994).
- [9] K. M. Hill and J. Kakalios, *Phys. Rev. E* **52**, 4393 (1995).
- [10] N. Jain, D. V. Khakhar, R. M. Lueptow, and J. M. Ottino, *Phys. Rev. Lett.* **86**, 3771 (2001).
- [11] S. J. Fiedor and J. M. Ottino, *Phys. Rev. Lett.* **91**, 244301 (2003).
- [12] J. F. Gilchrist and J. M. Ottino, *Phys. Rev. E* **68**, 061303 (2003).
- [13] T. Arndt, T. Siegmund-Hegerfeld, S. J. Fiedor, J. M. Ottino, and R. M. Lueptow, *Phys. Rev. E* **71**, 011306 (2005).
- [14] P. A. Cundall and D. L. Stack, *Géotechnique* **29**, 47 (1979).
- [15] P. Chen, J. M. Ottino, and R. M. Lueptow, *Phys. Rev. E* **78**, 021303 (2008).
- [16] G. H. Ristow, *Pattern Formation in Granular Materials* (Springer-Verlag, Berlin, 2000).
- [17] D. C. Rapaport, *Phys. Rev. E* **65**, 061306 (2002).
- [18] N. Taberlet, M. Newey, P. Richard, and W. Losert, *J. Stat. Mech.* (2006) P07013.
- [19] K. M. Hill, A. Caprihan, and J. Kakalios, *Phys. Rev. Lett.* **78**, 50 (1997).
- [20] L. Naji and R. Stannarius, *Phys. Rev. E* **79**, 031307 (2009).